WILEY | Hindawi

Research Article

Enhancement of the Thermohydraulic Performance in a Double Passage Square Duct with the Use of Inclined Ribs of 45°: A Comparative Computational Study

Mahmut Kaplan (ID)

Gaziantep University, Gaziantep 27600, Türkiye

Correspondence should be addressed to Mahmut Kaplan; mahmutkaplan@gantep.edu.tr

The modern gas turbines need to run at very high inlet temperature to promote their power output. Thus, improvements in cooling technologies play a significant role for enhancing the gas turbine blade life. In this paper, thermohydraulic performance (THP) of a two-pass square channel with inclined ribs at 45° was scrutinized employing the $k-\varepsilon$ realizable model with enhanced wall treatment in ANSYS Fluent. The calculations were performed for the rib pitch to height ratio (p/e) of 5-10, rib height to hydraulic diameter ratio (e/D_h) of 0.1-0.2, and Reynolds number (Re) of 20,000-40,000. Detailed analysis of the flow structure in a double passage square duct was carried out to understand the interaction of the rib and bend-induced secondary flows and its contribution to heat transfer enhancement for the rib configurations with distinct p/e and e/D_h, which was not available in any other existing numerical or experimental investigations. The results revealed that the ribs with higher e/D_h generated the stronger stream-wise secondary flows which led to the augmentation of the cooling performance with the disadvantage of pressure loss increment. The maximum THP of 26.55% was achieved with the ribbed configuration having $p/e = 5$ and $e/D_h = 0.1$ at Re = 20,000. The new correlations were developed from the computational data to predict the normalized Nusselt number and friction factor (Nu/Nu_0 and f/f_0, where 0 is the correlation), taking the e/D_h and flow Re into consideration.

1. Introduction

Gas turbines have a variety of applications such as aircraft, marine, and locomotive propulsion; electric power generation; and industrial uses. High operating temperature (above 2000 K) is required to elevate thermal efficiency and output capability of this century's gas turbines [1]. But temperature in the turbine is far beyond the blade material-softening temperature which will create extreme thermal stress owing to metallurgical constraints, and thus, there is a need to limit the temperature to prevent blade failure [2]. Advances in cooling techniques play a vital role to prolong the turbine blade lifetime [3]. The blades are cooled using the coolant air. Internal cooling is attained by passing cooling gas within the blade passages and removing the heat from them.

Rib turbulators cast on the passage walls are used to decrease the blade surface temperature with increasing the turbulence level immediately near the wall in the serpentine channels [4]. The presence of ribs leads to breaking the laminar sublayer adjacent to the blade surfaces and generating local turbulence by separating and reattaching the flow. Therefore, using ribs in the channel reduces thermal resistance and thus increases heat transfer from the passage surfaces to the coolant.

The ribs are characterized by various geometrical features such as rib shape, rib height (e), the distance between ribs known as pitch (p), attack angle (α), and rib orientation. The geometrical features of the ribs significantly affect flow mixing and heat transfer performance. Ribs of various shapes like rectangular, square, triangular, semicircular,

circular, and elliptical are used to cool the blade. Agrawal et al. [5–8] searched experimentally distinct discrete double-arc rib configurations with different arc angles of 30°-75°, a fixed rib height to hydraulic diameter ratio ($e/D_h = 0.027$), and the rib pitch to height ratio ($p/e = 6.67 - 11.67$) at Reynolds number (Re) of 3000-14000. They noticed that an increase in Re led to a considerable enhancement in Nusselt number with a decrease of friction factor (f). Thermohydraulic performance (THP) reached the peak value for $p/e = 8.33$ at an arc angle of 60° [5–8]. Sahu et al. [9] analyzed the impact of triangular, semicircular, and hybrid (the combination of triangular and semicircular) cross-section ribs on THP in a channel with aspect ratio (AR) of 4 : 1 and $p/e = 6.6 - 53.3$ at Re = 12640 − 52410. The maximum THP was achieved with hybrid cross-section ribs at $p/e = 13.3$.

Ribs can be located orthogonal or at angle to flow direction in the channel. Angled ribs developing cross-stream secondary flows contribute to promoting fluid mixing and heat transfer in the ducts. It was observed that the Nusselt number ratio in the ribbed channel with $\alpha = 30°$, 45°, and 60° were higher than that with $\alpha = 90°$ owing to the flow separation and reattachment along the ribs [1].

Recent numerical studies [10–23] have concentrated on the secondary flow triggered by ribs orientated 45° and their influences on heat transfer. Lei et al. [12] examined the influences of p/e on the thermal performance in a rotating two-pass channel with an AR = 2 : 1. They indicated that the heat transfer augmented with reducing p/e at stationary condition. Siddique et al. [14] conducted a numerical study to scrutinize THP of a 45°-angled ribbed channel with AR = 1 : 3 in the first pass and AR = 1 : 1 in the second pass and the sharp 180° bend. It was found that the pressure loss in the channel with AR = 1 : 3 was less than that with AR = 1 : 2 in the inlet pass [13] and pressure drop reduced with rising the distance of divider-to-tip wall. Gao et al. [16] simulated the secondary flow behavior and heat transfer characteristic of air and steam in a 45°-ribbed channel with AR = 4 : 1 and $e/D_h = 0.078$ at Re = 10, 000 − 60,000. They noticed that the secondary flow formation, separation, and mixing over the ribbed wall intensified the strength of local heat transfer.

Ravi et al. [17] numerically evaluated the friction and heat transfer features of 45°, M, V, and W ribs in a two-pass stationary channel with a fixed p/e of 16 and e/D_h of 0.125, and they reported that the overall THP of 45° and V ribs were better than those of the M and W ribs. Gong et al. [19] observed the distribution of heat transfer in a duct having 45° oblique ribs truncated continuously and discontinuously on one side with certain truncated lengths of 1.9, 3.8, and 5.7 mm at Re = 10, 000 − 60,000. The findings indicated that the case of ribs truncated continuously at 3.8 mm increased average Nusselt number and THP by 24.6% and 17.8%, respectively. Gong et al. [20] numerically predicted thermohydraulic behavior of mist/steam in the square channels with distinct orientations of 45° angled at Re = 10, 000 − 60,000. They pointed out that secondary flow structures in the channel were greatly dependent on rib orientations and THP of mist/steam coolant in the channels was much higher than that with steam ones due to the presence of water droplets, especially at higher Re.
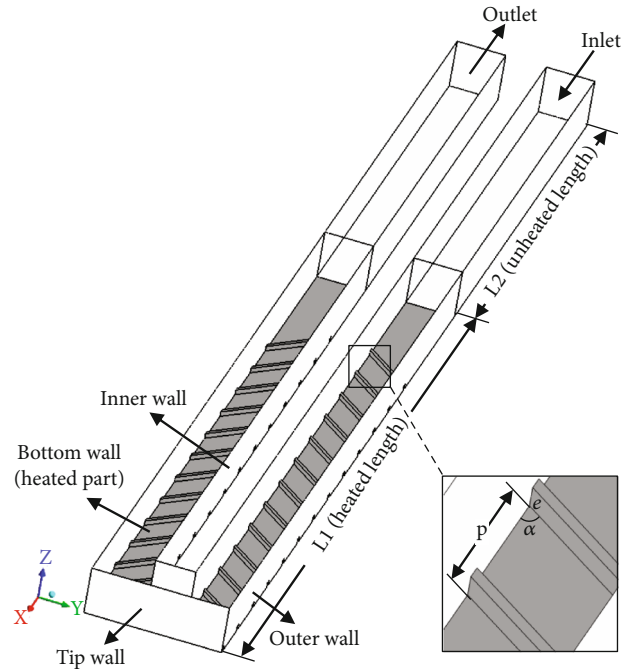

FIGURE 1: Schematic of the ribbed channel and geometrical parameters.
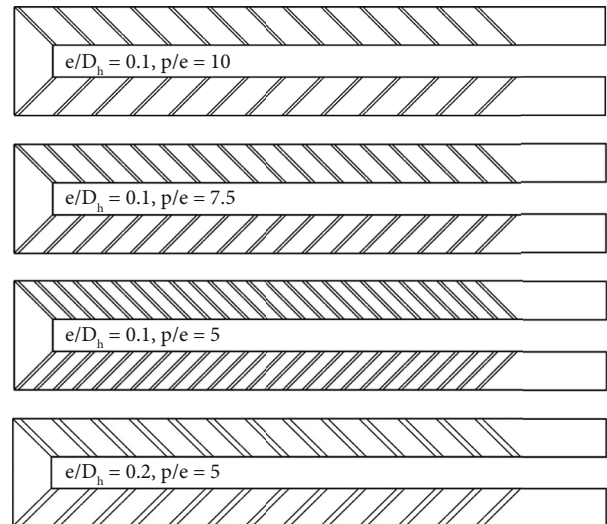

FIGURE 2: Ribbed channel configurations.

Tanda and Satta [21] scrutinized thermohydraulic efficiency of a 5:1 channel with standard, one central, and two equally spaced intersecting 45°-angled ribs for Re = 10,000 and 20,000. Their CFD results illustrated that the presence of single or double intersecting ribs induced additional vortex which contributed to elevate the friction and heat transfer in comparison to the standard inclined rib case. Zhang et al. [23] performed a CFD study on the effect of 45°-inclined a-quarter-cylinder, petal-shaped, and square ribs for a fixed cross-section area and rib height on THP in a two-passage channel. It was concluded that the ribs having curved surfaces improved turbulent mixing and THP.
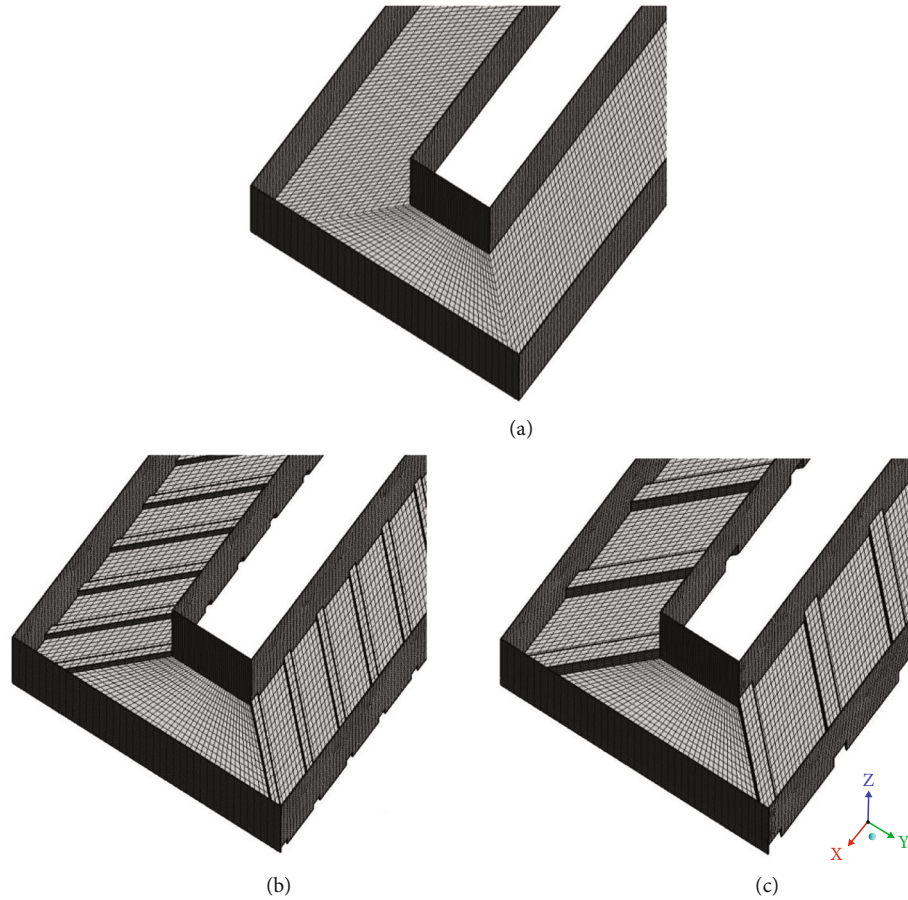
(a)

(b)

(c)

FIGURE 3: Mesh structure of channel configurations: (a) smooth, (b) $e/D_h = 0.1$, and (c) $e/D_h = 0.2$.

Literature studies showed that using 45°-inclined ribs is a common practice to elevate heat transfer in the turbine blade channels at the cost of further pressure loss and THP of a square channel was strongly affected by variations of rib spacing and height. The current work focuses on the influences of 45°-angled ribs having p/e of 5-10 and e/D_h of 0.1-0.2 on the flow pattern and THP in a square channel at Re $= 20,000 - 40,000$ employing ANSYS Fluent.

The detailed analysis of secondary flows produced by 180° bend and 45° ribs is limited in the literature. The current study provides new knowledge and insight into secondary vortical structure in the turn and ribbed walls. The study is aimed at understanding the relationship between strength of secondary flows and geometrical parameters of ribs to augment heat transfer performance and minimize pressure drop in the channel. The present computational work can be useful for the design engineers and researchers to better comprehend fluid flow and heat transfer mechanism in the ribbed channel.

2. Computational Procedure

The steps of the three-dimensional (3D) CFD model preparation, computational parameters, and model validity are described in detail in this section.
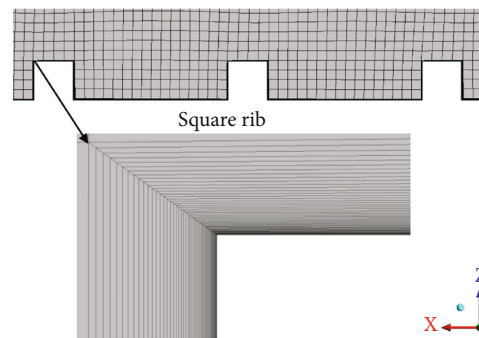

FIGURE 4: The inflation grid structure near the bottom wall.

TABLE 1: $y+$ value at the heated bottom wall for various configurations for Re = 30,000.

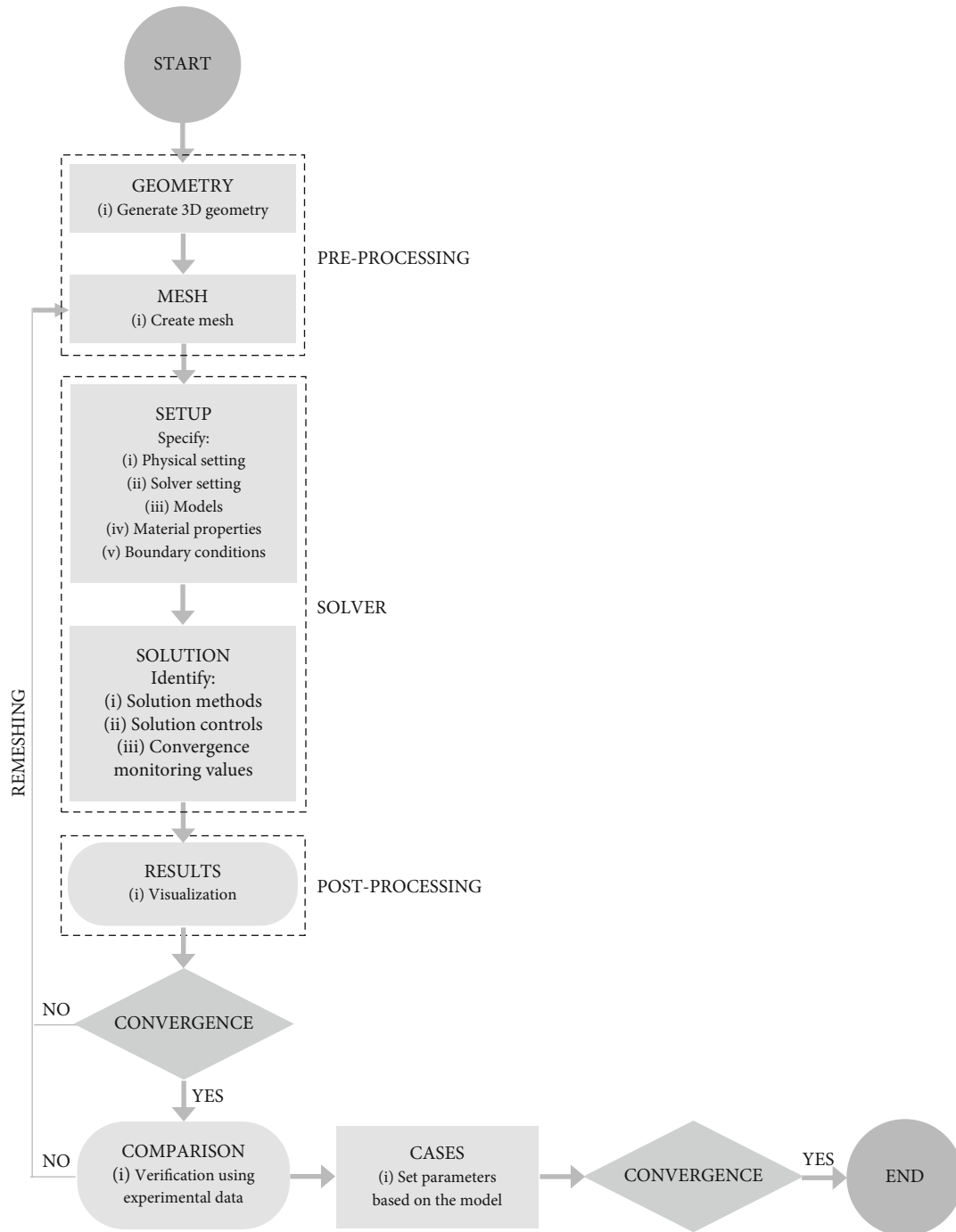| e/D_h	p/e	$y+$
0.1	5	0.0353
0.1	7.5	0.0332
0.1	10	0.0334
0.2	5	0.0392
Smooth		0.0231

FIGURE 5: Flowchart of CFD simulation procedure for the smooth and ribbed channel configurations.

2.1. Description of Physical Model.

Figure 1 displays the schematic view of a 45°-angled ribbed channel with a 24 mm × 24 mm cross section.

The dimensions of the channel used in the work in Figure 1 are similar to those used by Erelli et al.'s experimental study [24].

The bottom wall is heated, whereas all other walls are adiabatic. The heated part length (L_1) containing the turn area is 370 mm. The length of the unheated entrance part (L_2) is 210 mm. L_2 is required to get the fully developed flow.

The first and second passages are separated by the divider wall with 20 mm thickness. The four different 45°-angled ribbed channels are produced by locating square cross-section ribs with various rib spacings ($p/e = 5 - 10$) and rib heights ($e/D_h = 0.1 - 0.2$) on the bottom (heated part) wall of both two passes in Figure 2.

2.2. Mesh Generation and Computational Settings.

The geometry of the smooth and ribbed channels was created by using ANSYS DesignModeler and the hexahedral mesh

of the geometry was created by using Meshing in ANSYS Workbench. The grids of the smooth and ribbed channel configurations at $p/e = 5$ are illustrated in Figure 3.

The CFD simulation was conducted with ANSYS Fluent. Erelli et al. [24] employed different turbulence models (the standard and SST $k - \omega$ and the standard, realizable, and RNG $k - \varepsilon$) to predict heat transfer of the smooth channel whose dimensions considered in this study. They reported that the realizable $k - \varepsilon$ model gave better estimations than others.

The turbulence in the channel was thus estimated by employing the realizable $k - \varepsilon$ model integrating with enhanced wall treatment [25] in the CFD simulation. It is a near wall modelling based on enhanced wall functions with a two-layer model.

In this method, the mesh size near the wall should be fine to provide that $y+$ value is less than 1 [26]. Therefore, in this study, 52 inflation layers were generated at the bottom wall to keep the $y+$ below 1 for all configurations in Figure 4.

The area averaged $y+$ values at the bottom wall for the configurations are remarkably lower than one shown in Table 1.

The mesh growth rate of 1.2 was specified for the transition layers. The computation was considered converged when the residuals reached 10^{-5}. For the solution method, the steady pressure-based coupled algorithm was used and pseudo transient was selected to improve the rate of solution convergence. The gradient was calculated by least squares cell-based approach which was less expensive in terms of the simulation time. The second-order upwind scheme was utilized to discretize the equations.

2.3. Boundary Conditions. In the present work, the cooling air characteristics are considered to be fixed and not temperature dependent. The flow is three-dimensional, steady and turbulent. The velocity inlet and outflow are selected at the inlet and outlet of all configurations. The inlet velocity is uniform. It is calculated using Reynolds numbers. The inlet temperature is 299.48 K. Since the channel geometry involves 180° sharp turn and rib-roughened surfaces, the turbulent intensity is considered to be higher, and thus, 10% turbulent intensity is specified at the inlet. The nonslip and stationary wall conditions are applied on the walls. A fixed heat flux (q) of 2773 W/m^2 [24] is applied on the bottom wall. All other walls are unheated.

The numerical study is performed using the steps outlined in the flowchart in Figure 5.

2.4. Definition of Parameters. Reynolds number (Re) is calculated as

$$\mathrm{Re} = \frac{\rho V D_h}{\mu}, \tag{1}$$

where ρ, V, and μ are the density, velocity, and dynamic viscosity of air, respectively, and D_h is the channel hydraulic diameter. The local heat transfer coefficient (h) is described as
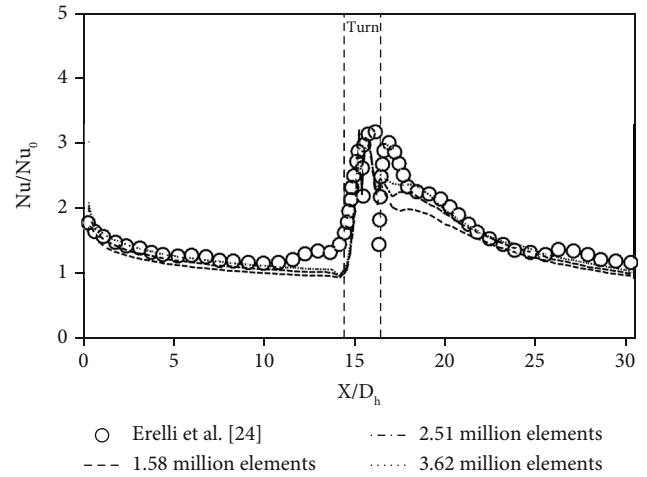

FIGURE 6: The span-wise averaged Nusselt number ratios for three grids and measured data along the flow direction at Re = 30,000.

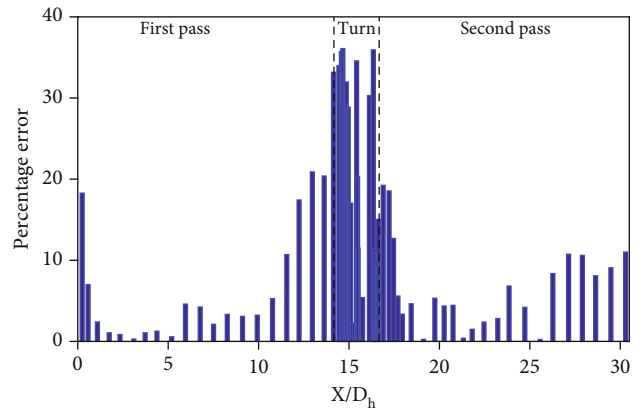FIGURE 7: Bar graph of the percentage error for fine grid.

$$h = \frac{q}{T_w - T_b}, \tag{2}$$

where T_b and T_w are the cooling air bulk mean and heated wall temperatures. The Nusselt number (Nu) is computed by

$$\mathrm{Nu} = \frac{h D_h}{k}, \tag{3}$$

where k is the thermal conductivity of air. The Dittus and Boelter equation [27–29] is utilized to normalize the Nusselt number.

$$\mathrm{Nu}_0 = 0.023 \, \mathrm{Re}^{0.8} \mathrm{Pr}^{0.4}, \tag{4}$$

where 0 denotes the correlation. The friction factor is computed by [30]

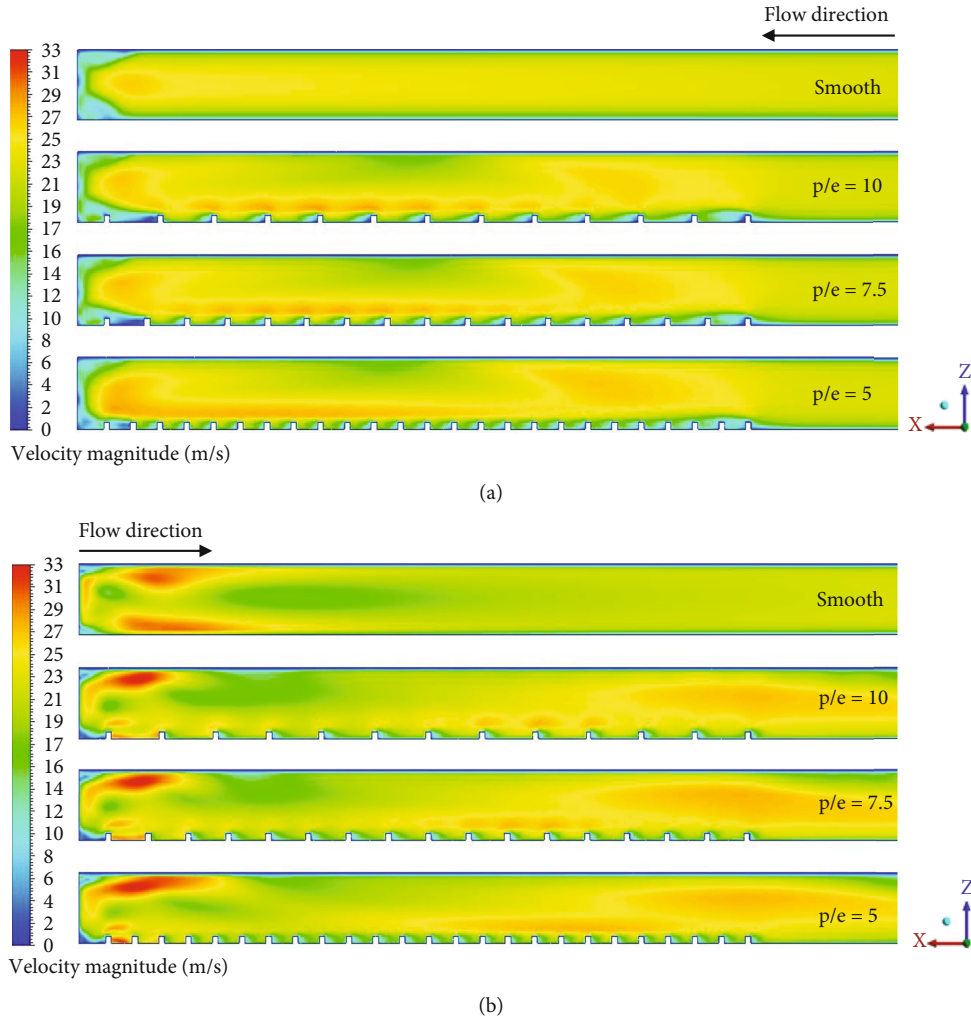$$f = \frac{\Delta P D_h}{2\rho V^2 L}, \tag{5}$$

(a)

(b)

FIGURE 8: Velocity magnitude distribution at the planes in the middle between the inner and outer walls for (a) first pass and (b) second pass of the smooth and ribbed channels ($p/e = 5 - 10$ and $e/D_h = 0.1$) at Re = 30,000.

where ΔP is the difference between the inlet and outlet pressures and L is the channel length crossing the centerline between inlet and outlet. Friction factor (f) is normalized employing the Blasius correlation [31]:

$$f_0 = \frac{0.046}{\mathrm{Re}^{0.2}}. \tag{6}$$

THP is calculated by [10]

$$\mathrm{THP} = \left(\frac{\mathrm{Nu}/\mathrm{Nu}_0}{f/f_0}\right)^{1/3}. \tag{7}$$

2.5. Grid Independence Study and Validation. Three grid sizes, namely, coarse (1.58 million), medium (2.51 million), and fine (3.62 million), are generated to ensure the mesh-independent solution. Figure 6 demonstrates a comparison

of Nusselt number ratios for the grids and Erelli et al.' measured data [24] at Re = 30,000. They evaluated the maximum uncertainty in Nusselt number to be approximately 8.2%, whereas the friction factor was measured with uncertainty of ±0.3% [24].

The results of the coarse grid are remarkably different; then, the results produced the medium and the fine grids which are quite close to the measured data in both passages.

The percentage error of the predicted Nusselt number ratio is calculated using the following equation:

$$\mathrm{Percentage\ error} = \frac{\left|(\mathrm{Nu}/\mathrm{Nu}_0)_{\mathrm{measured}} - (\mathrm{Nu}/\mathrm{Nu}_0)_{\mathrm{predicted}}\right|}{(\mathrm{Nu}/\mathrm{Nu}_0)_{\mathrm{measured}}} \times 100. \tag{8}$$

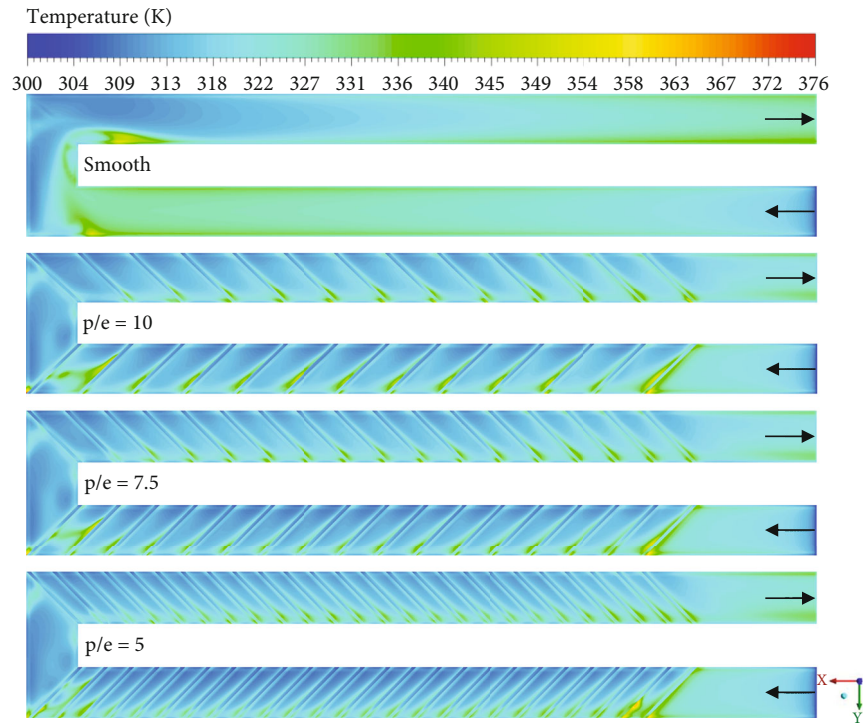Figure 7 shows the percentage error bar graph for the fine grid.

FIGURE 9: Temperature distribution on the heated wall for the smooth and ribbed channels ($p/e = 5 - 10$ and $e/D_h = 0.1$) at Re = 30,000.

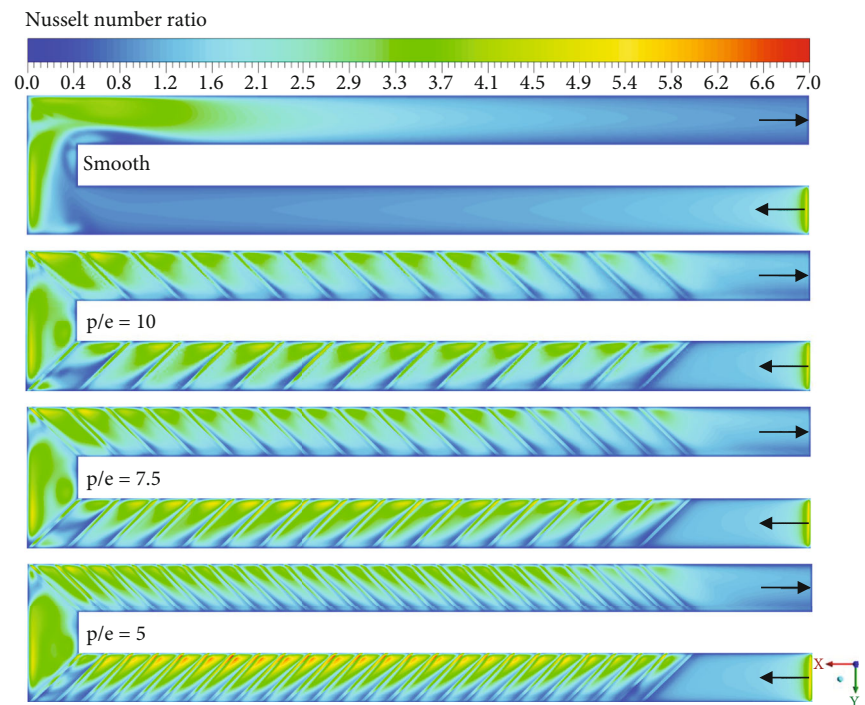

FIGURE 10: Nusselt number ratio distribution on the heated wall for the smooth and ribbed channels ($p/e = 5 - 10$ and $e/D_h = 0.1$) at Re = 30,000.

The percentage error bar graph obtained using MATLAB indicates that the errors in the prediction of Nusselt number ratios augmented in the turn region compared to the first and second pass. Therefore, the peak percentage error of 35.9% is gained in the bend region, whereas the minimum percentage error of 0.2 is achieved in the second pass.

The root mean square error (RMSE) and coefficient of determination (R^2) are utilized to compare the estimated and experimental Nusselt number ratio values for the fine grid:

$$\text{RMSE} = \sqrt{\frac{1}{n}\sum_{i=1}^{n}\left(\left(\frac{\text{Nu}}{\text{Nu}_0}\right)_{\text{measured}} - \left(\frac{\text{Nu}}{\text{Nu}_0}\right)_{\text{predicted}}\right)^2}, \quad (9)$$

$$R^2 = 1 - \frac{\sum_{i=1}^{n}\left((\text{Nu}/\text{Nu}_0)_{\text{measured}} - (\text{Nu}/\text{Nu}_0)_{\text{predicted}}\right)^2}{\sum_{i=1}^{n}\left((\text{Nu}/\text{Nu}_0)_{\text{measured}} - \overline{(\text{Nu}/\text{Nu}_0)}_{\text{measured}}\right)^2}, \quad (10)$$

where $\overline{\text{Nu}/\text{Nu}_0}$ is the average value of measured data.

The lower RMSE values of 0.16 and 0.21 are obtained for the first and second passes, while higher value of 0.59 is obtained for the turn. R^2 values are 0.71, 0.46, and 0.91 for the first pass, turn, and second pass. Like the percentage error, higher RMSE and lower R^2 indicate that the model prediction ability is poor in the turn region. This is due to the inability of the model to predict anisotropic turbulence causing a sudden shift in heat transfer in the turn.

Since the fine grid indicates considerably good agreement with the experiment [24], this grid is selected for the calculation. The number of division used the smooth channel is set to edges of the ribbed channels.

3. Result and Discussion

In this section, thermal and hydraulic performance of various 45° rib configurations with varying rib spacings and rib heights in a two-passage square channel is discussed.

3.1. Impact of p/e on the Thermohydraulic Characteristics. Figure 8 illustrates the velocity magnitude contours at the plans in the middle between the outer and inner walls for the first and second passes of the smooth and ribbed channels ($p/e = 5 - 10$ and $e/D_h = 0.1$) at Re = 30,000. It is observed in Figure 8 that velocity increases with decreasing rib spacing in both passages of ribbed channels compared to smooth channel.

Thus, the flow accelerates near the rib regions, which leads to enhancing fluid mixing [32]. Due to 180° bend and the divider wall, the stronger secondary flows are generated around the bend area of the smooth and ribbed channels. The higher velocity results in enhancing turbulence level and flow mixing in the bend.

The intensity of secondary flows produced by the turn diminishes gradually in the outlet passage of the smooth configuration. But in the ribbed configurations, the secondary flows developed by 45° ribs interact with that induced by the bend and the existence of the ribs results in increasing velocity in the downstream of the turn in Figure 8(b).

Figures 7 and 8 illustrate temperature and Nusselt number ratio contours on the heated wall of the smooth and ribbed channels, respectively. There is a considerable reduc-

TABLE 2: The calculated results at Re = 30,000.

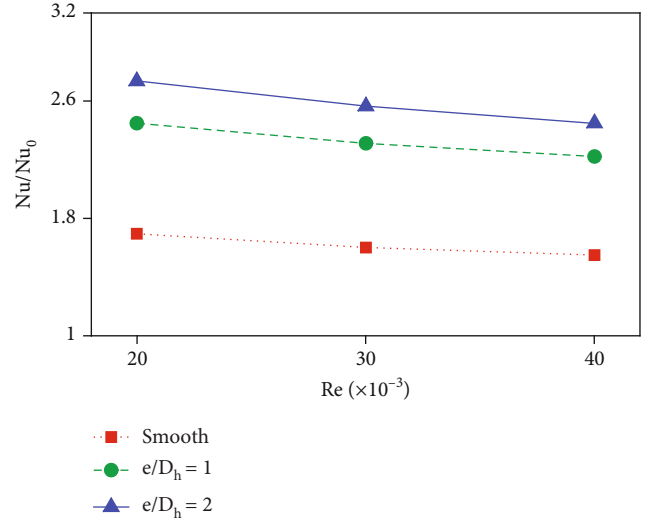| Configurations	Nu/Nu_0	f/f_0	THP
Smooth	1.60	2.82	1.13
$p/e = 5$	2.31	5.34	1.32
$p/e = 7.5$	2.20	5.32	1.26
$p/e = 10$	2.12	5.12	1.23

FIGURE 11: Nusselt number ratio versus Re for the smooth and ribbed configurations.

tion in temperature in the ribbed channels in comparison to the smooth one in Figure 9.

Besides, the ribbed surface temperature decreases with a decrease in p/e, especially in the first pass. It is owing to a rise in velocity near the rib regions in Figure 8. This leads to an improvement in heat exchanging between the coolant air and ribbed bottom wall in Figure 9. Thus, a remarkable decrease of temperature on the ribbed wall is observed for both the first and second passes in Figure 9. The interference between secondary flows generated by the bend and ribs also causes reducing temperature of the heated wall in the bend region.

It is apparent in Figure 10 that the Nusselt number ratio distribution on the smooth channel-heated surface shows a significant change with the addition of 45° ribs. The ribbed configurations enhance cooling performance in comparison to the smooth channel in Figure 10. A decrease in p/e augments Nusselt number ratio, especially in the first pass.

Meanwhile, in the bend of ribbed channels, the Nusselt number distribution is more uniform owing to interacting secondary flows formed by the bend and ribs in Figure 10.

Nusselt number ratio diminishes gradually in the second pass since the impact of secondary flow reduces in the smooth channel. But a continued rise in the Nusselt number ratio through the outlet pass is observed with the ribbed configurations since secondary flows are formed by ribs, as shown in Figure 10.
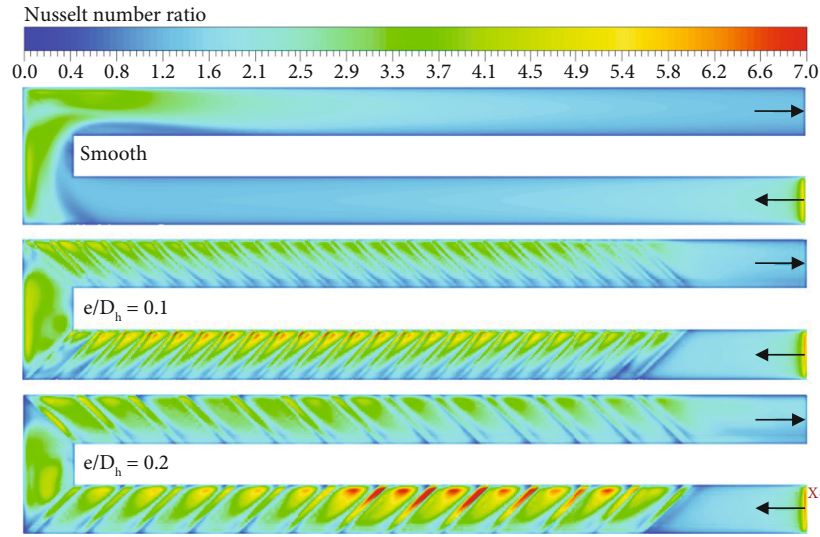
FIGURE 12: Nusselt number ratio distribution on the heated wall for the smooth and ribbed channels at Re = 20,000.

Table 2 illustrates the Nusselt number ratio, friction factor ratio, and THP for distinct configurations at Re = 30,000.

As shown in Table 2, Nusselt number ratio enhances with decreasing in the p/e. It is obvious that the friction of ribbed configurations is remarkably higher than the smooth one in Table 2. The friction factor augments with a decrease p/e from 10 to 7.5. On the other hand, the friction factor remains nearly constant for $p/e < 7.5$. Therefore, the ribbed channel having $p/e = 5$ and $e/D_h = 0.1$ ensures better heat transfer augmentation and increases THP by 16.81% compared to the smooth one.

3.2. Impact of e/D_h on the Thermohydraulic Characteristics. In this section, since the maximum THP is obtained with the ribbed configuration having $p/e = 5$ in Table 2, the impact of the rib height ($e/D_h = 0.1 - 0.2$) on the thermohydraulic features is examined at $p/e = 5$ for $Re = 20,000 - 40,000$.

The verification of the CFD simulation is made at Re = 30,000. Thus, the range of Re is selected according to lower and higher than this value to understand the effect of turbulent flow over rib-roughened surfaces on the friction and heat transfer.

Figure 11 demonstrates the Nusselt number ratio plotted with Re for the smooth and ribbed configurations. It is seen that increasing e/D_h results in higher Nusselt number ratio for $Re = 20,000 - 40,000$ in Figure 11. Besides, Nusselt number ratio enhances with a decrease in Re.

As a general trend, increasing Re promotes the heat transfer. But, since Nusselt number ratio predicted in the CFD simulation is lower than that calculated using Dittus-Boelter equation, the peak Nusselt number ratio of 2.74 is attained with $e/D_h = 0.2$ and $p/e = 5$ for Re = 20,000.

Using the regression analysis of commercial software of MATLAB, the Nu/Nu_0 correlation as a function of e/D_h and Re is improved based on the computational data gained employing ANSYS Fluent in Figure 11 and the value of R^2 is 0.98.

$$\frac{Nu}{Nu_0} = (e/D_h)^{0.155}\left(2.667 + 1.15 \times 10^{-5}\, Re\right). \quad (11)$$

Ravi et al. obtained the maximum Nusselt number ratio of approximately 1.82, 1.98, 2.25, and 2.45 for the M, W, 45°, and V ribbed channels with $p/e = 16$ and $e/D_h = 0.125$ for Re = 19,500, respectively. In comparison to Ravi et al.'s results, the configuration generated with a decrease in p/e and an increase in e/D_h augments Nusselt number ratio considerably at for Re = 20,000. Therefore, the Nusselt number ratio distribution on the heated wall of the smooth and ribbed channels ($e/D_h = 0.1 - 0.2$, $p/e = 5$) is examined for Re of 20,000 in Figure 12.

Nusselt number ratio augments with increasing e/D_h from 0.1 to 0.2, especially near the inner wall of the inlet pass and outer wall of the outlet pass owing to the stronger secondary flow associated with higher velocity in this region in Figure 12.

As the flow accelerates with increasing the rib height, stronger flow impingement occurring on the surface of the ribs promotes heat transfer. Therefore, higher thermal performance is obtained with ribbed channel with $e/D_h = 0.2$ for Re = 20,000.

To provide more insight into the relationship between the heat transfer and secondary flow structure, three different planes are examined at Re = 20,000 in Figure 13.

Planes 1 and 3 are located at 48 mm ($2 \times D_h$) from the tip wall in the first and second passes of the channel, respectively, and plane 2 is located at the midsection of the turn.

These planes are observed by a watcher travelling flow direction in the channel.

Figure 14 indicates velocity vectors plotted at the selected planes in the smooth and ribbed configurations.

At plane 1, a secondary flow vortex is not produced in the smooth channel. But a vortex rotating in clockwise direction is generated by ribbed configurations in Figure 14(a). It is evident that increasing e/D_h from 0.1 to 0.2 leads to
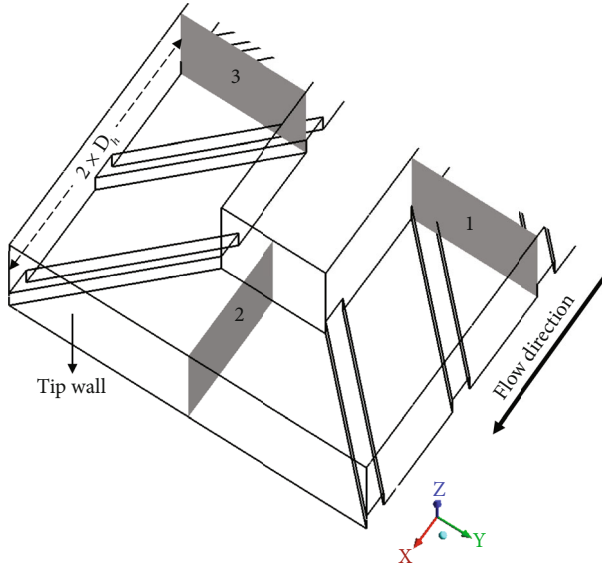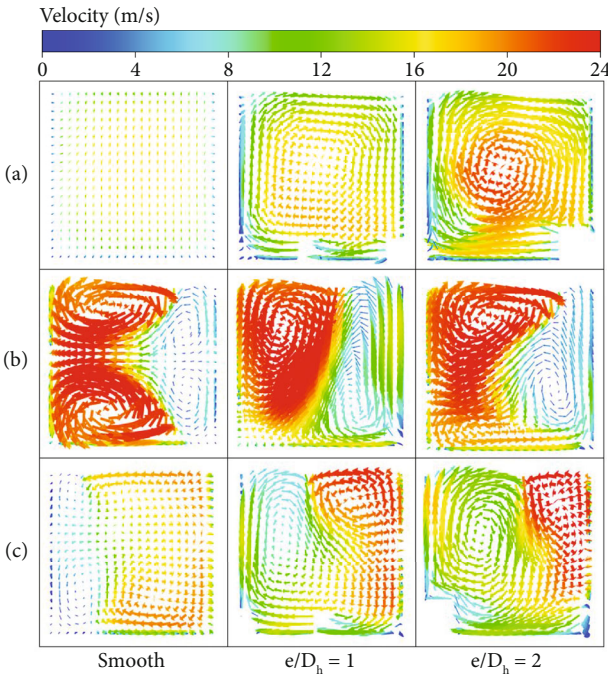
FIGURE 13: Velocity vector planes.

FIGURE 14: Secondary flow vectors at (a) plane 1, (b) plane 2, and (c) plane 3 at Re = 20,000.

FIGURE 15: Friction factor ratio versus Re for the smooth and ribbed channels ($p/e = 5$, $e/D_h = 0.1 - 0.2$).

increasing the intensity of the vortex and velocity near the heated wall in Figure 14(a).

At plane 2, two strong and two weaker counter-rotating vortices are produced, thanks to the bend in the smooth channel in Figure 14(b). But, owing to the impact of the turn and ribs, two and three counter-rotating vortices are produced by ribbed configurations with e/D_h of 0.1 and 0.2, respectively.

It is found that high pressure at outer wall and the centrifugal force as a result of the sharper turning of the flow improve vortex structure at plane 2 (the middle of the bend).
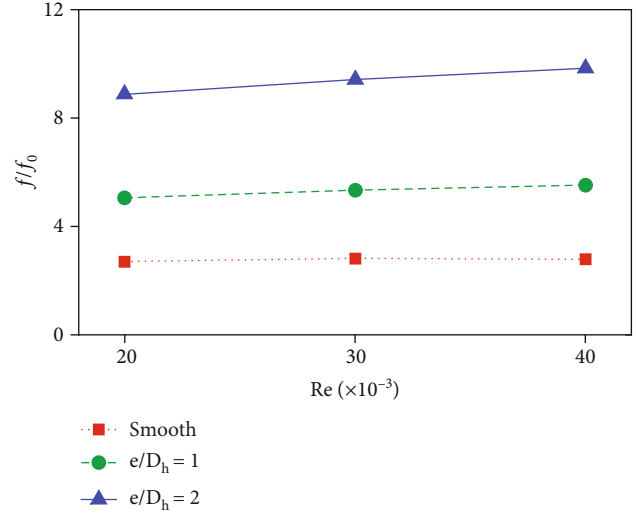
At plane 3, the impact of secondary flows developed by the bend is reduced in the smooth channel, whereas in the ribbed channels, two counter-rotating vortices are produced owing to the existence of ribs in Figure 14(c). Increasing rib height from 0.1 to 0.2 enhances the flow velocity near the rib region in Figure 14(c).

Figure 15 illustrates the friction factor ratio plotted with Re for the smooth and ribbed configurations.

The elevated rib height promotes the friction compared with the smooth channel for Re = 20,000 − 40,000 in Figure 15. The impact of the rib height on friction factor ratio is much stronger for the ribbed configuration with $e/D_h = 0.2$.

The peak friction factor ratio of 9.84 is attained with $e/D_h = 0.2$ and $p/e = 5$ for Re = 40,000. Ravi et al. gained the friction factor ratio of approximately 7.6, 8.2, 8.8, and 10 for the M, W, 45°, and V ribbed channels with $p/e = 16$ and $e/D_h = 0.125$ for Re = 35,500, respectively.

Figure 16 demonstrates THP plotted with Re for the channel configurations.

THP is significantly augmented by the ribbed configurations in Figure 16. It is noticed that the friction factor ratio in Figure 15 is a dominant factor for enhancing THP. The maximum THP of 26.55% is obtained with the ribbed configuration having $e/D_h = 0.1$ at $p/e = 5$. Thus, this configuration can be a promising option for the improvement of cooling performance of ribbed channels in gas turbines.

Using first-order polynomial regression analysis of commercial software of MATLAB, the f/f_0 correlation as a function of e/D_h and Re is improved based on the calculation data obtained using ANSYS Fluent in Figure 16 and $R^2 = 0.98$.

$$\frac{f}{f_0} = (e/D_h)^{0.821}\left(4.604 + 2.35 \times 10^{-5}\ \text{Re}\right). \quad (12)$$

The main conclusion in this section is that the rib height should be limited due to pressure drop increment
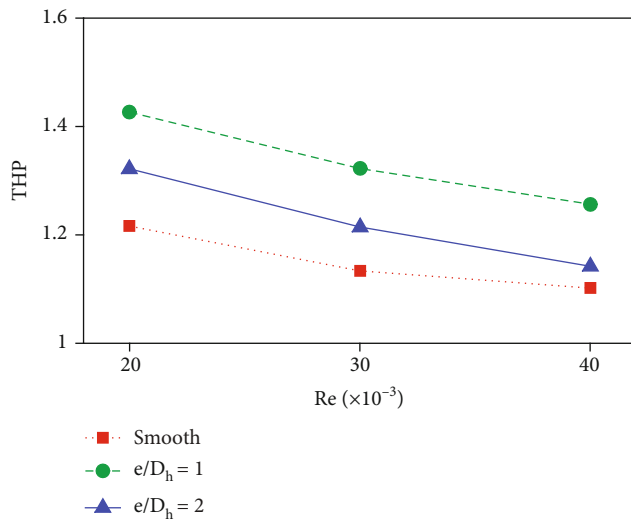
FIGURE 16: THP versus Re for the smooth and ribbed channels ($p/e = 5$, $e/D_h = 0.1 - 0.2$).

and the geometrical features of ribs are very important to improve secondary flow structures and thus elevate THP of the ribbed channel.

4. Conclusions

In the current work, the combined influence of p/e and e/D_h on the thermal and hydraulic performance is evaluated computationally in a square channel consisting two passages having 45° ribs. The geometrical model was validated by the experiment [24]. The relevant conclusions are as follows:

(1) The 45°-angled ribbed channels significantly augment heat transfer performance at the expense of elevated friction factor in comparison to smooth channel

(2) Nusselt number ratio, flow velocity, and friction losses augment with decreasing p/e for a fixed rib height at Re = 30,000, while influence of p/e on pressure loss significantly diminishes for $p < 7.5$

(3) The secondary flow vortices induced by the bend and ribs enhance turbulent activity near the heated surface and thus improve thermal performance

(4) Increasing e/D_h for a constant p/e further enhances secondary flow structures and heat transfer but produces higher pressure drop at Re = 20, 000 − 40, 000

(5) The rib height has a more marked influence on the friction factor than rib spacing. The highest Nusselt number ratio of 2.74 was obtained with the ribbed channel having $e/D_h = 0.2$ and $p/e = 5$ due to higher velocity enhancing flow impingement on the ribbed surface compared to other configurations

(6) The configuration having $e/D_h = 0.1$ and $p/e = 5$ is a good choice regarding higher pressure loss in the

ribbed channel, and this configuration increases THP by 26.55% compared to the smooth one

(7) New correlations were developed to estimate Nu/Nu$_0$ and f/f_0 as a function of e/D_h and flow Re

The findings of this research study can be useful for researchers, designers, and engineers to understand the interaction between secondary flow structures, pressure drop, and heat transfer features of the gas turbine blade internal coolant passage with the ribs.

Nomenclature

D_h: Hydraulic diameter
e: Rib height
f: Friction factor
h: Heat transfer coefficient
k: Thermal conductivity
L: Length
Nu: Nusselt number
Pr: Prandtl number
$\dot{q}$: Heat flux
Re: Reynolds number
T: Temperature
V: Velocity
X: Distance in the stream-wise direction.

Greek Letters

μ: Dynamic viscosity
ρ: Density.

Subscripts

0: Correlation
b: Bulk
w: Wall.

Abbreviations

CFD: Computational fluid dynamics
THP: Thermohydraulic performance.

Data Availability

The author confirms that the data supporting the findings of this work are available within the article.

Conflicts of Interest

The author declares no potential conflicts of interest concerning the publication of this article.

References

[1] J. C. Han, S. Dutta, and S. V. Ekkad, *Gas Turbine Heat Transfer and Cooling Technology*, CRC Press, Boca Raton, 2nd edition, 2012.

[2] T. S. Chowdhury, F. T. Mohsin, M. M. Tonni, M. N. H. Mita, and M. M. Ehsan, "A critical review on gas turbine cooling

performance and failure analysis of turbine blades," *International Journal of Thermofluids*, vol. 18, article 100329, 2023.

[3] G. Zhang, R. Zhu, G. Xie, S. Li, and B. Sunden, "Optimization of cooling structures in gas turbines: a review," *Chinese Journal of Aeronautics*, vol. 35, no. 6, pp. 18–46, 2022.

[4] B. Sunden and G. Xie, "Gas turbine blade tip heat transfer and cooling: a literature survey," *Heat Transfer Engineering*, vol. 31, no. 7, pp. 527–554, 2010.

[5] Y. Agrawal and J. L. Bhagoria, "Experimental investigation for pitch and angle of arc effect of discrete artificial roughness on Nusselt number and fluid flow characteristics of a solar air heater," *Materials Today: Proceedings*, vol. 46, pp. 5506–5511, 2021.

[6] Y. Agrawal, J. L. Bhagoria, and V. S. Pagey, "Enhancement of thermal efficiency of solar air collector by using discrete double arc reverse shaped roughness on the absorber plate," *Materials Today: Proceedings*, vol. 51, pp. 1548–1553, 2022.

[7] Y. Agrawal, J. L. Bhagoria, A. Gautam et al., "Experimental evaluation of hydrothermal performance of solar air heater with discrete roughened plate," *Applied Thermal Engineering*, vol. 211, article 118379, 2022.

[8] Y. Agrawal, J. L. Bhagoria, A. Gautam et al., "Investigation of thermal performance of a ribbed solar air heater for sustainable built environment," *Sustainable Energy Technologies and Assessments*, vol. 57, article 103288, 2023.

[9] M. K. Sahu, K. M. Pandey, and S. Chatterjee, "Thermohydraulic performance of rectangular channel roughened with combined semi-circular and triangular ribs," *Heat and Mass Transfer*, vol. 55, no. 10, pp. 2889–2900, 2019.

[10] P. Singh, Y. Ji, and S. V. Ekkad, "Experimental and numerical investigation of heat and fluid flow in a square duct featuring criss-cross rib patterns," *Applied Thermal Engineering*, vol. 128, pp. 415–425, 2018.

[11] Z. Guo, Y. Rao, Y. Li, and W. Wang, "Experimental and numerical investigation of turbulent flow heat transfer in a serpentine channel with multiple short ribbed passes and turning vanes," *International Journal of Thermal Sciences*, vol. 165, article 106931, 2021.

[12] J. Lei, J. C. Han, and M. Huh, "Effect of rib spacing on heat transfer in a two pass rectangular channel (AR=2:1) at high rotation numbers," *ASME 2011 Turbo Expo: Turbine Technical Conference and Exposition*, 2011, Vancouver, British Columbia, Canada, 2011, 2011.

[13] I. V. Shevchuk, S. C. Jenkins, B. Weigand, J. V. Wolfersdorf, S. O. Neumann, and M. Schnieder, "Validation and analysis of numerical results for a varying aspect ratio two-pass internal cooling channel," *ASME Journal of Heat Transfer*, vol. 133, no. 5, article 051101, 2011.

[14] W. Siddique, I. V. Shevchuk, L. El-Gabry, N. B. Hushmandi, and T. H. Fransson, "On flow structure, heat transfer and pressure drop in varying aspect ratio two-pass rectangular channel with ribs at 45," *Heat and Mass Transfer*, vol. 49, no. 5, pp. 679–694, 2013.

[15] J. Park, S. Park, and P. M. Ligrani, "Numerical predictions of detailed flow structural characteristics in a channel with angled rib turbulators," *Journal of Mechanical Science and Technology*, vol. 29, no. 11, pp. 4981–4991, 2015.

[16] T. Gao, J. Zhu, C. Liu, and J. Xu, "Numerical study of conjugate heat transfer of steam and air in high aspect ratio rectangular ribbed cooling channel," *Journal of Mechanical Science and Technology*, vol. 30, no. 3, pp. 1431–1442, 2016.

[17] B. V. Ravi, P. Singh, and S. V. Ekkad, "Numerical investigation of turbulent flow and heat transfer in two-pass ribbed channels," *International Journal of Thermal Sciences*, vol. 112, pp. 31–43, 2017.

[18] T. Gao, J. Zhu, J. Li, J. Gong, and Q. Xia, "Improving heat transfer performance in two-pass ribbed channel by the optimized secondary flow via bend shape modification," *International Communications in Heat and Mass Transfer*, vol. 103, pp. 43–53, 2019.

[19] J. Gong, X. Zhang, J. Zeng, T. Gao, and W. Wu, "Experimental and numerical investigation of heat transfer characteristics in a square channel with various truncated ribs," *Journal of Mechanical Science and Technology*, vol. 33, no. 8, pp. 4029–4038, 2019.

[20] J. Gong, C. Ma, J. Lu, and T. Gao, "Effect of rib orientation on heat transfer and flow characteristics of mist/steam in square channels," *International Communications in Heat and Mass Transfer*, vol. 118, article 104900, 2020.

[21] G. Tanda and F. Satta, "Heat transfer and friction in a high aspect ratio rectangular channel with angled and intersecting ribs," *International Journal of Heat and Mass Transfer*, vol. 169, article 120906, 2021.

[22] X. Wang, H. Xu, J. Wang, W. Song, and L. Wang, "High pressure turbine blade internal cooling in a realistic rib roughened two-pass channel," *International Journal of Heat and Mass Transfer*, vol. 170, article 121019, 2021.

[23] Q. Zhang, T. Wang, Q. Z. Hou, K. W. Song, W. L. Hu, and X. Wu, "Thermal hydraulic performance augmentation by petal-shaped ribs in a two-pass cooling channel," *Case Studies in Thermal Engineering*, vol. 40, article 102542, 2022.

[24] R. Erelli, A. K. Saha, and P. K. Panigrahi, "Influence of turn geometry on turbulent fluid flow and heat transfer in a stationary two-pass square duct," *International Journal of Heat and Mass Transfer*, vol. 89, pp. 667–684, 2015.

[25] ANSYS, Inc, *ANSYS Fluent Theory Guide, Release 19.2*, ANSYS Inc., Canonsburg, PA, 2018.

[26] C. Liu, B. Li, L. Ye, H. Zhu, C. Zhang, and W. Song, "Film cooling characteristics of cross-flow coolant passage with various relative positions of holes and inclined ribs," *International Journal of Thermal Sciences*, vol. 167, article 106975, 2021.

[27] Y. Agrawal, J. L. Bhagoria, and V. S. Pagey, "Enhancement of thermo-hydraulic performance using double arc reverse ribs in a solar collector: experimental approach," *Materials Today: Proceedings*, vol. 47, pp. 6067–6073, 2021.

[28] Y. Agrawal, S. F. Ahmed, V. Mahate, and J. L. Bhagoria, "Augmentation of heat transfer and fluidity characteristics of rectangular solar air collector using discrete roughness elements on the absorber plate: an experimental analysis," in *International Symposium on Fluids and Thermal Engineering (FLUTE 2021)*, pp. 1–10, Noida, India, 2021.

[29] Y. Agrawal, K. Yugbodh, S. F. Ahmed et al., "Experimental investigation of heat transfer and flow analysis of artificially roughened solar air heater by using double arc reverse shaped roughness with gap on the absorber plate," *Materials Today: Proceedings*, vol. 78, pp. 403–413, 2023.

[30] Y. Agrawal, J. L. Bhagoria, K. Yugbodh, E. Jain, and A. Gautam, "Thermohydraulic performance of solar air heater having discrete double arc roughness elements on absorber plate," *Materials Today: Proceedings*, vol. 68, pp. 326–334, 2022.

[31] W. M. Kays, M. E. Crawford, and B. Weigand, *Convective Heat and Mass Transfer*, McGraw-Hill, Boston, 4th edition, 2005.

[32] S. S. Gajghate, O. P. Deshpande, A. U. Desai et al., "Effect of ribs configurations on heat transfer enhancement for W-shaped ribs in a square duct," *Arabian Journal for Science and Engineering*, vol. 48, no. 9, pp. 12141–12160, 2023.